Journal of Nuclear Medicine, published on December 14, 2018 as doi:10.2967/jnumed.118.221416

N-(2-(dimethylamino)ethyl)-4-^{18}F-fluorobenzamide: A Novel Molecular Probe for High-Contrast PET Imaging of Malignant Melanoma

Ayoung Pyo[1], Hyeon-Sik Kim[1], Gyeongmin Kim[1], Hyung-Seok Kim[2], Misun Yun[3],

Dong-Yeon Kim[1*], Jung-Joon Min[1*]

[1]*Department of Nuclear Medicine, Chonnam National University Medical School and Hwasun Hospital, Hwasun, Korea*
[2]*Department of Forensic Medicine, Chonnam National University Medical School, Hwasun, Korea*
[3] *Microbiology and Functionality Research Group, World Institute of Kimchi, Gwangju, Korea*

Address correspondence to: **Jung-Joon Min** (jjmin@jnu.ac.kr), **Dong-Yeon Kim** (blueburr@gmail.com)

Jung-Joon Min, M.D., PhD.
Department of Nuclear Medicine, Chonnam National University Medical School and Hwasun Hospital
160 Ilsimri, Hwasun, Jeonnam 519-763, Republic of Korea
Phone: 82-61-379-2876
Fax: 82-61-379-2875
E-mail: jjmin@jnu.ac.kr

Dong-Yeon Kim, PhD.
Department of Nuclear Medicine, Chonnam National University Medical School and Hwasun Hospital
160 Ilsimri, Hwasun, Jeonnam 519-763, Republic of Korea
Phone: 82-61-379-2872
Fax: 82-61-379-2875
E-mail: blueburr@gmail.com

Ayoung Pyo, PhD
Department of Nuclear Medicine, Chonnam National University Hwasun Hospital
160 Ilsimri, Hwasun, Jeonnam 519-763, Republic of Korea
Tel: 82-61-379-7262
Fax: 82-61-379-2875
E-mail: payjal@naver.com

Short running title: ^{18}F-DMFB for malignant melanoma

Total word count of the manuscript: 4954

Financial support: This research was supported by a Basic Science Research Program through the National Research Foundation of Korea (NRF), funded by the Ministry of Education (2017R1D1A1B03029055 and 2018R1A6A3A01012344), and by the Pioneer Research Center Program through the National Research Foundation of Korea, funded by the Ministry of Science, ICT & Future Planning (2015M3C1A3056410).

Disclosure: The authors have no competing interests to declare.

ABSTRACT

Malignant melanoma is a very aggressive and serious form of skin cancer, with prognosis and treatment outcome depending heavily on the clinical stage of the disease at the time of diagnosis. Here, we synthesized a novel ^{18}F-labeled benzamide derivative to target melanoma, and then evaluated its biological characteristics in small animal models.

Methods: *N*-(2-(dimethylamino)ethyl)-4-^{18}F-fluorobenzamide (^{18}F-DMFB) was synthesized by reaction of *N*-succinimidyl 4-^{18}F-fluorobenzoate with *N,N*-dimethylethylenediamine. The binding affinity of ^{18}F-DMFB was measured in B16F10 (mouse melanoma) cells with or without L-tyrosine. MicroPET imaging with ^{18}F-DMFB was performed in B16F10 xenograft and metastasis mouse models.

Results: The overall non-decay-corrected radiochemical yield of ^{18}F-DMFB was approximately 10%–15%. Uptake of ^{18}F-DMFB was melanin-specific as cellular uptake in B16F10 increased more than 18-fold in the presence of L-tyrosine. Biodistribution studies revealed that ^{18}F-DMFB accumulated, and was retained, in B16F10 xenografts for 120 min (10, 30, 60 and 120 min: 9.24, 10.80, 13.0, 10.59 %ID/g, respectively) of post-radiotracer injection. Liver uptake of ^{18}F-DMFB decreased from 10 to 120 min and showed fast clearance (10, 30, 60 and 120 min: 11.19, 5.7, 2.47, 0.4 %ID/g). Furthermore, ^{18}F-DMFB allowed visualization of metastatic lesions immediately after injection, and was retained in lesions for over 60 min, with a high tumor-to-background ratio.

Conclusion: ^{18}F-DMFB demonstrated high melanin targeting ability and tumor-specific tumor uptake in both primary and metastatic lesions in animal models bearing malignant melanoma. ^{18}F-DMFB may be a potential PET imaging agent for melanoma.

Key words: Malignant melanoma, Metastasis, ^{18}F-labeled benzamide derivative, PET, Molecular imaging

INTRODUCTION

Malignant melanoma is the most aggressive type of skin cancer, with the highest rates of metastasis and mortality (*1,2*). The incidence of metastatic melanoma has increased over the past three decades, with a mortality rate that continues to rise faster than that of most other cancers (*3*). In the last few years we have witnessed an unparalleled change in treatment options for patients with metastatic melanoma, including development of new therapeutic strategies like targeted therapies and immunotherapies, which have improved patient prognosis substantially. Despite the paradigm-shifting success of these novel treatments, their effectiveness is still limited by intrinsic or acquired resistance (*3*). Therefore, development of molecular imaging techniques able to precisely diagnose melanoma at the earliest practicable stage is crucial for improving the survival rate of patients with malignant disease (*4*).

Over recent decades, the imaging technologies of positron emission tomography (PET), single photon emission computed tomography (SPECT), magnetic resonance imaging (MRI), computed tomography (CT) and ultrasound have been studied in terms of their ability to detect melanoma. Of these, nuclear imaging technologies can visualize specific pathways or biomarkers of the melanoma disease process using molecular imaging probes. Several radiolabeled probes have been designed and evaluated for melanoma detection, including antibody-based imaging agents that show specific binding to melanoma, although technical limitations such as long residence time in the circulation and a slow penetration rate into the tumor were observed (*5,6*). *N*-isopropyl-*p*-^{123}I-iodoamphetamine (^{123}I-IMP) was developed originally to measure cerebral blood flow and used to diagnose cerebrovascular diseases like epilepsy and dementia. An unexpected benefit of ^{123}I-IMP is that after intravenous (*i.v.*) injection it is found in high concentrations in tissue regions producing melanin. However, detection of metastatic melanoma in the lungs and liver has proved difficult because ^{123}I-IMP shows high accumulation in these organs (*7-10*).

The benzamide structure has selective affinity for the pigment melanin, which is an irregular polymer produced by melanocytes (*11*). In malignant melanoma, the concentration of melanin increases substantially because elevated tyrosinase activity accelerates melanin biosynthesis. Many different radiolabeled benzamide derivatives have been investigated and reported for melanoma detection. During the initial stages of the research, ^{123}I or ^{125}I labeled benzamide derivatives were examined with respect to autoradiography or scintigraphy (*12-15*). These probes showed specific uptake by melanoma *in vivo*, revealing their potential as diagnostic probes. Following on from these, several ^{99m}Tc-complexes based on the structural elements of benzamide were reported for melanoma detection using SPECT (*16-19*). These probes were evaluated in B16 murine melanoma-bearing mice and showed tumor-specific uptake; however, improvements to their targeting ability were needed before they could be applied in clinical trials. In recent years, the PET radionuclides ^{68}Ga and ^{18}F, which provide higher spatial resolution, have been employed to radiolabel benzamide derivatives (*11,20-25*). Among them, ^{18}F-P3BZA was evaluated in melanoma patients as preliminary clinical application and suggests a potential use for melanoma diagnosis (*26*). The skeleton structures of these probes are benzamide and aliphatic structures, including an alkyl linker and amine residue.

Here, we report the synthesis and characterization of *N*-(2-(dimethylamino)ethyl)-4-^{18}F-fluorobenzamide (^{18}F-DMFB) for early detection of metastatic melanoma using PET. We modified the structure of the benzamide derivatives to improve its ability to target melanoma. Biological evaluations, including *in vitro* uptake, biodistribution, and microPET studies, were performed in both metastatic melanoma and primary tumor models. Finally, we demonstrated the superiority of ^{18}F-DMFB as a novel PET agent for detecting metastatic malignant melanoma.

MATERIALS AND METHODS

Synthesis of ^{19}F-DMFB

The synthesis scheme for ^{19}F-DMFB is shown in Supplemental Figure 1. *O*-(*N*-succinimidyl)-1,1,3,3-tetramethyl-uronium tetrafluoroborate (TSTU; 215 mg, 0.714 mmol) and *N,N*-diisopropylethylamine (DIPEA; 277 mg, 2.14 mmol) were added to a solution of 4-fluorobenzoic acid (100 mg, 0.714 mmol) in 5 mL of *N,N*-dimethylformamide. The reaction mixture was stirred for 3 h at 60°C and then cooled to room temperature. Subsequently, *N,N*-dimethylethylenediamine (DMEA; 107 mg, 1.21 mmol) was added to the reaction mixture. After stirring at room temperature for 2 h, the mixture was treated with H_2O and extracted with dichloromethane. After evaporation of the solvent, the crude mixture was purified using silica gel chromatography [dichloromethane (MC):methanol (MeOH) = 10:1] and obtained as a yellow oil to yield 132 mg (88%) of ^{19}F-DMFB. ^{1}H nuclear magnetic resonance (NMR) (300 MHz, chloroform-d) δ (ppm) 2.23 (s, 6H), 4.48 (t, 2H, J = 3.6 Hz), 3.47 (q 2H), 7.0 (br, 1H), 7.04 (m, 3H), 7.79 (m, 2H). ^{13}C NMR (75 MHz, chloroform-d) δ (ppm) 37.2, 45.1, 57.7, 115.4 (J = 12.75 Hz), 129.3 (J = 5.25 Hz), 130.7 (J = 2.25 Hz), 164.6 (J = 150 Hz), 166.4. High-resolution mass spectrometry (Fast atom bombardment) *m/z* calculated for $C_{11}H_{15}FN_2O$ $[M+H]^+$ = 211.1247; actual = 211.1246.

Radiolabeling of ^{18}F-DMFB

The chemical structures and synthesis scheme for ^{18}F-DMFB are shown in Figure 1 and Supplemental Figure 2. The *N*-succinimidyl-4-^{18}F-fluorobenzoate (^{18}F-SFB) was prepared as described previously, with some modifications (*27*). Briefly, DMEA (7.6 mg, 86 μmol) was added to a solution of ^{18}F-SFB in 0.2 mL of dimethyl sulfoxide. After stirring at 60°C for 30 min, the solution was cooled and injected into a semi-preparative high-performance liquid chromatography column system for purification. The mobile phase started with 100% solvent A (0.1% trifluoroacetic acid in water) and 0% solvent B (0.1%

trifluoroacetic acid in acetonitrile) and ramped to 40% solvent A and 60% solvent B at 30 min; flow rate = 3 mL/min [retention time (R_t): 16.15 min].

Stability Study and In Vitro Binding Assay

The stability of ^{18}F-DMFB was analyzed by modification of a previously reported method (*28*). ITLC-sg strips developed with MC and MeOH (10 : 1) and were scanned. *In vitro* binding assay were performed as previously described (*23*).

Cell Culture and Cellular Uptake Studies

B16F10 (mouse melanoma), U87MG (human glioblastoma) and CT26 (mouse colon) cells were cultured in DMEM (B16F10, U87MG) or RPMI (CT26) supplemented with 10% FBS. Cellular uptake studies were performed and calculated as previously described method (*24*).

Preparation of Animal Models and Biodistribution Studies

Animal care, animal experiments, and euthanasia were performed in accordance with protocols approved by the Chonnam National University Animal Research Committee and the Guide for the Care and Use of Laboratory Animals (*29*). For the subcutaneous tumor models, Foxn1nu mice (5–6 weeks old) were injected in the shoulder with B16F10 (1×10^6) cells, CT26 cells (1×10^6), or U87MG cells (1×10^7). The lung metastases were created in C57BL/6 mice (5–6 weeks old) *via i.v.* injection of B16F10 cells (2×10^5). The lymph node (LN) metastasis models were generated by injection of B16F10 cells (2×10^5 in 50 μl DPBS) into the footpad of Foxn1nu mice for 2 min. The biodistribution studies in different organs were conducted 10, 30, 60, and 120 min after *i.v.* injection of 7.4 MBq of ^{18}F-DMFB into B16F10-bearing mice (n = 3 / each time point, tumor size: 100-150 mm^3).

Small Animal PET

MicroPET images were obtained using a high-resolution small animal PET-SPECT-CT scanner (Inveon, Siemens Medical Solutions). MicroPET studies of the tumor models (tumor size: 100-150 mm^3) were performed using *i.v.* injection of ^{18}F-DMFB (7.4 MBq); images were acquired for 10 min. To compare ^{18}F-DMFB and 2-deoxy-2-^{18}F-fluoro-D-glucose (^{18}F-FDG) images of melanoma, mouse models were injected with ^{18}F-DMFB 1 day after ^{18}F-FDG PET imaging. Regions of interest (ROI) were drawn over the tumor, liver and muscle on decay-corrected coronal images and analyzed. Acquired images were reconstructed with a three dimensional ordered subset expectation maximization (OSEM3D) algorithm and image analysis was performed with PMOD software (PMOD Technologies Ltd, Zürich, Switzerland) (*30,31*). Uptake value was expressed as %ID/g in coronal and transaxial PET images.

Statistical Analysis

The Mann-Whitney U-test was used for statistical analysis. A P value of < 0.05 was considered statistically significant. All data are expressed as the mean ± standard deviation.

RESULTS

Tracer Preparation and In Vitro Stability

^{19}F-DMFB was synthesized *via* one-step procedures between 4-fluorobenzoic acid and DMEA. The cold form was separated by silica gel chromatography and analyzed by ^{1}H, ^{13}C NMR, and high-resolution mass spectrometry to confirm its identity (Supplemental Fig. 2). The chemical yield of ^{19}F-DMFB was 75%. Different from cold synthesis, ^{18}F-DMFB was generated *via* coupling of the ^{18}F prosthetic group ^{18}F-SFB to DMEA. The total labeling time of the ^{18}F-DMFB was within 140 min, including separation using high-performance liquid chromatography and the overall decay-corrected RCY was approximately 15%–30%. The identity of ^{18}F-DMFB was confirmed by comparing the retention times with that of the reference compound (Supplemental Fig. 3). The specific activity of ^{18}F-DMFB was greater than 5.5 GBq/μmol. When the radiotracer was incubated in human serum at 37 ℃ for 2 h, the percentage of the remaining ^{18}F-DMFB (R_f, 0.15–0.20) was greater than 95% (Supplemental Fig. 4).

In Vitro Binding and Cellular Uptake Studies

The binding affinity of ^{18}F-DMFB for melanin was assessed using commercial synthetic melanin (Fig. 2A). ^{18}F-DMFB showed high binding affinity for melanin (approximately 90%) at 10 min post-treatment, with binding retained for up to 2 h (86.84 ± 0.48%). Cell uptake studies of ^{18}F-DMFB were performed in the B16F10 cell line at 37℃ for 1 h. Treatment with L-tyrosine (2 mM) stimulated the B16F10 cells and changed their color to black, with these black cells then being considered as “activated” melanoma cells. Compared to inactivated B16F10 cells, the activated cells showed rapid and high accumulation of ^{18}F-DMFB at 10 min (1.84 ± 0.07% *vs.* 0.20 ± 0.06%), with uptake increasing for 1 h (2.28 ± 0.55% *vs.* 0.12 ± 0.01%) (Fig. 2B).

In Vivo Biodistribution Studies

The *in vivo* biodistribution of ^{18}F-DMFB was examined in B16F10 tumor-bearing Foxn1nu mice at 10, 30, 60 and 120 min post-*i.v.* injection of ^{18}F-DMFB. A high level of radioactivity accumulated in the tumors, while activity in organs showed rapid washout. Tumor uptake of ^{18}F-DMFB was > 9 %ID/g at 10 min post-radiotracer injection, and 13 %ID/g at 1 h (Table 1). The tumor-to-skin, -lung, -brain, -liver, -bone and -intestine ratios were 6.54 ± 1.02, 7.13 ± 2.44, 12.20 ± 5.00, 5.54 ± 1.27, 13.73 ± 5.87, and 4.90 ± 0.22, respectively at 1 h post-^{18}F-DMFB injection (Supplemental Table. 1). Notably, these ratios increased to at least 20-fold at 2 h post-radiotracer injection.

MicroPET Imaging Studies of ^{18}F-DMFB

Static MicroPET studies of ^{18}F-DMFB were performed in B16F10-bearing Foxn1nu mice, as well as in CT26 or U87MG xenografts. B16F10 tumors could be visualized clearly at 10 min post-injection, and tumor uptake increased for 1 h, with excellent tumor-to-background contrast (7.39 ± 0.89 %ID/g at 1 h, Fig. 3A). A point of note is that there was no uptake in lung and liver after 30 min. In addition, only B16F10 tumors were specifically visualized when microPET studies were performed with B16F10 (8.49 %ID/g) and CT26 (0.85 %ID/g), or B16F10 (8.34 %ID/g) and U87MG (0.83 %ID/g), cell-bearing Foxn1nu mice (Fig. 3B and 3C).

In microPET imaging studies of the lung metastasis models, good visualization of the metastatic region was obtained 1 h after *i.v.* injection of ^{18}F-DMFB. Representative maximum intensity projection (MIP) and axial images of normal and metastatic mouse models collected between 60 and 70 min post-^{18}F-DMFB injection are shown in Figure 4A and 4B. ROI analysis showed that normal lung uptake of ^{18}F-DMFB was 0.53 ± 0.13 %ID/g, whereas uptake in lung metastasis was 6.58 ± 1.63 %ID/g (n = 11, P < 0.001, Supplemental Fig. 5). Furthermore, 1.93 mm-sized liver metastasis of melanoma was incidentally visualized by ^{18}F-DMFB PET (Fig. 4C).

On the basis of the microPET imaging results from lung metastasis models, we further investigated the ability of ^{18}F-DMFB to visualize LNs harboring metastatic malignant melanoma in mouse models. LN metastasis models were established in Foxn1nu mice by direct injection of B16F10 cells into the foot pad. Twenty-one days after cancer cell injection, over 70% of the mice had black-colored LNs in the popliteal area (Fig. 5A). As shown in Figure 5B, small metastatic popliteal LNs (< 4 mm) were clearly visualized by ^{18}F-DMFB PET, with a high signal-to-background ratio. Finally, metastatic LNs were confirmed by histopathologic analysis (Fig. 5C). Furthermore, we evaluated the sensitivity of ^{18}F-DMFB to metastatic popliteal LNs of different sizes. All LN metastases (size range: 1–7.5 mm; n = 5) were homogeneously visualized by ^{18}F-DMFB, regardless of tumor size (Supplemental Fig. 6).

Finally, we compared PET images of ^{18}F-DMFB and ^{18}F-FDG in B16F10-bearing Foxn1nu mice and lung metastasis models. B16F10 tumors were visualized clearly by each radiotracer at 60 min after i.v. injection; however, different patterns of biodistribution were observed (Fig. 6A). ^{18}F-DMFB accumulated in tumors and was otherwise rapidly washed out through the bladder, while ^{18}F-FDG showed uptake in brain, heart, liver, tumor, and bladder. The tumor-to-liver uptake ratios of ^{18}F-DMFB and ^{18}F-FDG at 60 min were 8.04 ± 0.81 and 5.04 ± 1.43, respectively (n = 9, $P < 0.01$), whereas the tumor-to-muscle uptake ratios were 15.21 ± 1.58 and 13.03 ± 2.40, respectively (n = 9, $P < 0.05$). Similar patterns were shown for PET imaging of each tracer in the lung metastasis models. Lung metastases imaged by ^{18}F-DMFB showed excellent metastasis-to-background contrast, while metastases were not prominent on ^{18}F-FDG imaging because of high background activity in brown adipose tissue and heart (Fig. 6B).

DISCUSSION

Metastasis is a representative characteristic of malignant melanoma and is the cause of the majority of melanoma-related deaths. The survival rate of malignant melanoma depends on the extent of the disease; if the malignant melanoma is localized, 5-year survival is 90%; however, if the tumor has metastasized at the time of diagnosis, 5-year survival is only 6%. Thus, accurate diagnosis of the tumor location at an early stage is crucial for increasing the probability of survival. In this study, we synthesized a novel ^{18}F labeled benzamide derivative to target melanin with high affinity, and evaluated its *in vitro* and *in vivo* performance.

Benzamide derivatives for PET are composed of radiolabeled benzamide and an aliphatic structure that includes an alkyl linker and an amine residue (*11,21-25,32,33*). Many researchers have modified the structure, especially the benzene ring, to improve RCY, melanin targeting ability, or pharmacokinetic properties. Although RCY was improved, biodistribution studies in mice show that melanoma uptake of these PET probes is less than 10 %ID/g at 60 min. Instead, we focused on the amine residue of the benzamide derivatives because melanin can be targeted by aliphatic structures like the *N,N*-diethylethylenediamine group (*34*). Finally, we changed the amine residue from ethyl to methyl, which resulted in high sensitivity for melanoma detection.

Our cellular and *in vivo* results indicate that ^{18}F-DMFB has good potential as a molecular probe to detect melanoma, with high stability and specificity. The *in vivo* biodistribution study revealed rapid and high accumulation of ^{18}F-DMFB in the tumor, with stable retention for at least 2 h. Previously, *N*-[2-(diethylamino)-ethyl]-4-^{18}F-fluorobenzamide, which has a benzamide structure with a diethyl amine residue, showed approximately 6 %ID/g tumor uptake at 1 h post-injection (*11,25*). However, ^{18}F-DMFB showed 2-fold higher tumor uptake than the previous compound at 1 h (13.00 ± 3.90 %ID/g). Rapid washout from all examined organs, but not from the tumor, resulted in high tumor-to-organ ratios. Tumor-to-skin, -lung, -liver, -bone and -intestine ratios are particularly important when developing a PET

agent for malignant melanoma because these organs are common sites for metastasis (*35*). Interestingly, brain uptake of ^{18}F-DMFB was observed at 1 and 2 h after injection (1.21 ± 0.70, 0.26 ± 0.08 %ID/g, respectively), which means that ^{18}F-DMFB can penetrate the blood-brain barrier. Previous publications reported that in B16F10-bearing mice, the tumor-to-brain ratio of ^{18}F-FDG was 2.86 ± 0.35 at 1 h (*11*). However, the tumor-to-brain ratio of ^{18}F-DMFB reached over 12 because of the low normal-brain uptake of ^{18}F-DMFB; this result demonstrates the potential of ^{18}F-DMFB for imaging of melanoma brain metastases.

In this respect, ^{18}F-DMFB has excellent *in vivo* properties as a PET probe to diagnose malignant melanoma. The biodistribution results were confirmed by microPET imaging, with tumors becoming visible about 10 min after ^{18}F-DMFB injection, and uptake continuing to increase up until 1 h. Melanin specificity was also confirmed by PET imaging in non-melanoma-bearing Foxn1nu mice.

A main goal of the present study was to investigate the feasibility of ^{18}F-DMFB for detecting melanoma metastasis. This was evaluated using murine models of lung, liver, and LN metastasis. We found that uptake of ^{18}F-DMFB was more than 12-fold higher in metastatic lung than in normal lung. The tumor-to-lung or tumor-to-liver ratios of ^{18}F-DMFB were very high in the biodistribution study, and a small liver metastasis was clearly visualized at 1 h on microPET imaging, with fast washout from the liver. Comparison studies of ^{18}F-DMFB and ^{18}F-FDG revealed that the tumor uptake value of ^{18}F-DMFB was lower than that of ^{18}F-FDG. However, the biodistribution of ^{18}F-DMFB was better than that of ^{18}F-FDG, which resulted in excellent tumor-to-background contrast. In particular, detection of lung metastases is difficult on ^{18}F-FDG PET because they can be masked by high uptake in the heart.

In addition, ^{18}F-DMFB demonstrated clear detection of LN metastasis. Regional LN status is the most important prognostic factor for malignant melanoma patients because the lymphatic system is invariably involved in spreading melanoma (*36,37*). Tumor cells enter a lymphatic vessel, transit through a LN, and then enter the systemic circulation *via* the thoracic duct (*35*).

In the present study, we demonstrated the excellent image quality of ^{18}F-DMFB for detecting primary and metastatic melanoma. However, it is reported that picolinamide derivatives show higher performance for malignant melanoma than benzamide derivatives (*4*). Therefore, we think that picolinamide derivatives with a dimethyl amine residue may show better performance with respect to diagnosis of metastatic malignant melanoma.

CONCLUSION

^{18}F-DMFB was easily synthesized *via* a coupling reaction and its *in vitro* and *in vivo* characteristics were evaluated. The rapid and prolonged retention of ^{18}F-DMFB in melanoma, but not in normal organs, suggests that this labeled probe can be used as an imaging agent to obtain high-contrast PET images of melanoma shortly after its injection. The excellent *in vivo* kinetics and specific tumor uptake warrant its further investigation for imaging of melanoma, with ^{18}F-DMFB having the potential to be a novel molecular probe for the PET-based diagnosis of malignant melanoma and its metastasis.

ACKNOWLEDGMENT

We thank Hwa Youn Jang (Innovation Center for Molecular Probe Development) for his excellent research assistance.

REFERENCES

1. Garbe C, Peris K, Hauschild A, et al. Diagnosis and treatment of melanoma. European consensus-based interdisciplinary guideline - Update 2016. *Eur J Cancer.* 2016;63:201-217.

2. Harries M, Malvehy J, Lebbe C, et al. Treatment patterns of advanced malignant melanoma (stage III-IV) - A review of current standards in Europe. *Eur J Cancer.* 2016;60:179-189.

3. Henriques V, Martins T, Link W, Ferreira BI. The emerging therapeutic landscape of advanced melanoma. *Curr Pharm Des.* 2018;24:549-558.

4. Liu H, Liu S, Miao Z, et al. Development of ^{18}F-labeled picolinamide probes for PET imaging of malignant melanoma. *J Med Chem.* 2013;56:895-901.

5. Vavere AL, Butch ER, Dearling JL, et al. ^{64}Cu-*p*-NH_2-Bn-DOTA-hu14.18K322A, a PET radiotracer targeting neuroblastoma and melanoma. *J Nucl Med.* 2012;53:1772-1778.

6. Voss SD, Smith SV, DiBartolo N, et al. Positron emission tomography (PET) imaging of neuroblastoma and melanoma with ^{64}Cu-SarAr immunoconjugates. *Proc Natl Acad Sci U S A.* 2007;104:17489-17493.

7. Ito Y, Doi H, Tsuji H, Ishida-Yamamto A, Iizuka H. Malignant melanoma of the breast: *N*-isopropyl-*p*-^{123}I-iodoamphetamine single photon emission computed tomography (^{123}I-IMP SPECT) is useful for the detection of metastasis. *J Dermatol.* 2010;37:849-851.

8. Yoshimura M, Kanesaka N, Saito K, Koizumi K, Tokuuye K, Goto H. Diagnosis of uveal malignant melanoma by a new semiquantitative assessment of *N*-isopropyl-*p*-[^{123}I]-iodoamphetamine. *Jpn J Ophthalmol.* 2011;55:148-154.

9. Sou R, Oku N, Ohguro N, Hibino S, Fujikado T, Tano Y. The clinical role of *N*-isopropyl-*p*-[^{123}I]-iodoamphetamine single photon emission computed tomography in the follow-up of choroidal melanoma after radiotherapy. *Jpn J Ophthalmol.* 2004;48:54-58.

10. Holman BL, Wick MM, Kaplan ML, et al. The relationship of the eye uptake of *N*-isopropyl-*p*-[^{123}I]iodoamphetamine to melanin production. *J Nucl Med.* 1984;25:315-319.

11. Ren G, Miao Z, Liu H, et al. Melanin-targeted preclinical PET imaging of melanoma metastasis. *J Nucl Med.* 2009;50:1692-1699.

12. Michelot JM, Moreau MF, Labarre PG, et al. Synthesis and evaluation of new iodine-125 radiopharmaceuticals as potential tracers for malignant melanoma. *J Nucl Med.* 1991;32:1573-1580.

13. Maffioli L, Mascheroni L, Mongioj V, et al. Scintigraphic detection of melanoma metastases with a radiolabeled benzamide ([iodine-123]-(S)-IBZM). *J Nucl Med.* 1994;35:1741-1747.

14. Michelot JM, Moreau MF, Veyre AJ, et al. Phase II scintigraphic clinical trial of malignant melanoma and metastases with iodine-123-*N*-(2-diethylaminoethyl 4-iodobenzamide). *J Nucl Med.* 1993;34:1260-1266.

15. Nicholl C, Mohammed A, Hull WE, Bubeck B, Eisenhut M. Pharmacokinetics of iodine-123-IMBA for melanoma imaging. *J Nucl Med.* 1997;38:127-133.

16. Auzeloux P, Moreau MF, Papon J, et al. Technetium-99m radiolabelling of an *N*-amino-alkyl-benzamide nitrido- and oxo-technetium bis(aminoethanethiol) derivative synthesis and biological results. Potential melanoma tracer agents. *J Labelled Comp Radiopharms.* 1999;42:567-579.

17. Auzeloux P, Papon J, Masnada T, et al. Synthesis and biodistribution of technetium-99m-labelled *N*-(diethylaminoethyl)benzamide via a bis(dithiocarbamate) nitridotechnetiuim(V) complex. *J Labelled Comp Radiopharm.* 1999;42:325-335.

18. Auzeloux P, Papon J, Azim EM, et al. A potential melanoma tracer: synthesis, radiolabeling, and biodistribution in mice of a new nitridotechnetium bis(aminothiol) derivative pharmacomodulated by a *N*-(diethylaminoethyl)benzamide. *J Med Chem.* 2000;43:190-198.

19. Auzeloux P, Papon J, Pasqualini R, Madelmont JC. Synthesis and biodistribution of a new oxo-technetium-99m bis(aminothiol) complex as a potential melanoma tracer. *J Med Chem.* 2001;44:1116-1121.

20. Kertesz I, Vida A, Nagy G, et al. In vivo imaging of experimental melanoma tumors using the novel radiotracer ^{68}Ga-NODAGA-procainamide (PCA). *J Cancer.* 2017;8:774-785.

21. Trencsenyi G, Denes N, Nagy G, et al. Comparative preclinical evaluation of ^{68}Ga-NODAGA and ^{68}Ga-HBED-CC conjugated procainamide in melanoma imaging. *J Pharm Biomed Anal.* 2017;139:54-64.

22. Chang CC, Chang CH, Lo YH, et al. Preparation and characterization of a novel Al^{18}F-NOTA-BZA conjugate for melanin-targeted imaging of malignant melanoma. *Bioorg Med Chem Lett.* 2016;26:4133-4139.

23. Kim HJ, Kim DY, Park JH, et al. Synthesis and characterization of a ^{68}Ga-labeled *N*-(2-diethylaminoethyl)benzamide derivative as potential PET probe for malignant melanoma. *Bioorg Med Chem.* 2012;20:4915-4920.

24. Kim HJ, Kim DY, Park JH, et al. Synthesis and evaluation of a novel ^{68}Ga-labeled DOTA-

benzamide derivative for malignant melanoma imaging. *Bioorg Med Chem Lett.* 2012;22:5288-5292.

25. Garg S, Kothari K, Thopate SR, Doke AK, Garg PK. Design, synthesis, and preliminary in vitro and in vivo evaluation of *N*-(2-diethylaminoethyl)-4-[^{18}F]fluorobenzamide ([^{18}F]-DAFBA): a novel potential PET probe to image melanoma tumors. *Bioconjug Chem.* 2009;20:583-590.

26. Ma X, Shengjun W, Wang S, et al. Biodistribution, radiation dosimetry, and clinical application of a melanin targeted PET probe ^{18}F-P3BZA in patients. *J Nucl Med.* May 31, 2018 [Epub ahead of print]

27. Tang G, Tang X, Wangb X. A facile automated synthesis of *N*-succinimidyl 4-[^{18}F]fluorobenzoate ([^{18}F]SFB) for ^{18}F-labeled cell-penetrating peptide as PET tracer. *J Label Compd Radiopharm.* 2010;53:543-547.

28. Yun M, Kim DY, Lee JJ, et al. A high-affinity repebody for molecular imaging of EGFR-expressing malignant tumors. *Theranostics.* 2017;7:2620-2633.

29. Garber JC, Barbee RW, Bielitzki JT, et al. *Guide for the Care and Use of Laboratory Animals 8th ed.* Washington, DC: The National Academies Press; 2011: 11-40. Accessed June 1, 2016.

30. Blasi F, Oliveira BL, Rietz TA, et al. Effect of chelate type and radioisotope on the imaging efficacy of 4 fibrin-specific PET probes. *J Nucl Med.* 2014;55:1157-1163.

31. Sah BR, Schibli R, Waibel R, et al. Tumor imaging in patients with advanced tumors using a new ^{99m}Tc-radiolabeled vitamin B12 derivative. *J Nucl Med.* 2014;55:43-49.

32. Denoyer D, Greguric I, Roselt P, et al. High-contrast PET of melanoma using ^{18}F-MEL050, a

selective probe for melanin with predominantly renal clearance. *J Nucl Med.* 2010;51:441-447.

33. Wu SY, Huang SP, Lo YC, et al. Synthesis and preclinical characterization of [^{18}F]FPBZA: a novel PET probe for melanoma. *Biomed Res Int.* 2014;2014:912498.

34. Liu HG, Liu SL, Miao Z, et al. A novel aliphatic ^{18}F-labeled probe for PET imaging of melanoma. *Mol Pharm.* 2013;10:3384-3391.

35. Damsky WE, Rosenbaum LE, Bosenberg M. Decoding melanoma metastasis. *Cancers (Basel).* 2010;3:126-163.

36. Pasquali S, Mocellin S, Campana LG, et al. Early (sentinel lymph node biopsy-guided) versus delayed lymphadenectomy in melanoma patients with lymph node metastases : personal experience and literature meta-analysis. *Cancer.* 2010;116:1201-1209.

37. Thomas JM. Sentinel lymph node biopsy in malignant melanoma. *BMJ.* 2008;336:902-903.

TABLES

Table 1. Biodistribution of ^{18}F-DMFB in Foxn1nu mice bearing B16F10 at 10, 30, 60 and 120 min after *i.v.* injection*

	10 min	30 min	60 min	120 min
Blood	5.26 ± 1.02	3.20 ± 0.51	0.98 ± 0.26	0.16 ± 0.006
Heart	6.22 ± 0.91	3.07 ± 0.17	1.20 ± 0.38	0.20 ± 0.024
Lung	11.66 ± 2.91	4.57 ± 0.65	1.89 ± 0.63	0.33 ± 0.031
Liver	11.19 ± 0.62	5.76 ± 0.41	2.47 ± 1.05	0.45 ± 0.06
Spleen	13.19 ± 2.58	5.88 ± 0.83	2.23 ± 0.92	0.34 ± 0.12
Stomach	9.01 ± 4.51	6.49 ± 2.35	2.87 ± 0.29	0.82 ± 0.64
Intestine	12.54 ± 1.56	7.88 ± 0.82	2.65 ± 0.80	0.52 ± 0.09
Kidney	40.42 ± 14.69	16.74 ± 4.91	5.08 ± 1.69	0.93 ± 0.29
Pancreas	10.03 ± 3.20	4.73 ± 0.62	1.77 ± 0.78	0.20 ± 0.05
Muscle	5.67 ± 0.60	3.36 ± 1.68	1.44 ± 0.11	0.34 ± 0.12
Bone	5.07 ± 0.38	2.40 ± 0.40	1.03 ± 0.47	0
Brain	6.84 ± 1.02	2.96 ± 0.61	1.21 ± 0.70	0.26 ± 0.08
Skin	7.73 ± 1.63	3.94 ± 1.73	1.96 ± 0.32	0.37 ± 0.07
Eyes	4.26 ± 0.50	2.79 ± 0.71	1.05 ± 0.07	0.04 ± 0.02
Tumor	9.24 ± 2.23	10.80 ± 3.27	13.00 ± 3.90	10.59 ± 1.35

* Data are expressed as %ID/g ± standard deviation (n = 3 / each time point).

FIGURE WITH LEGENDS

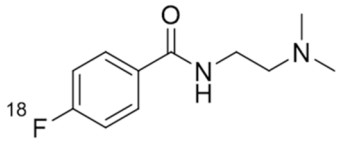

FIGURE 1. Chemical structure of ^{18}F-DMFB.

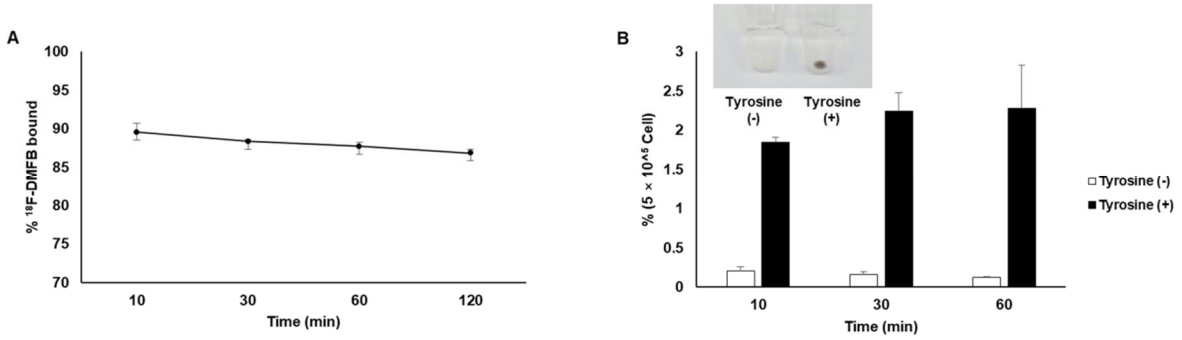

FIGURE 2. (A) *In vitro* binding of ^{18}F-DMFB to 2 mg melanin at 37℃ for 10, 30, 60 and 120 min. (B) *In vitro* uptake of ^{18}F-DMFB by B16F10 cells in the presence/absence of L-tyrosine at 10, 30 and 60 min, including a photograph of B16F10 cell pellets in the absence (left) or presence (right) of L-tyrosine.

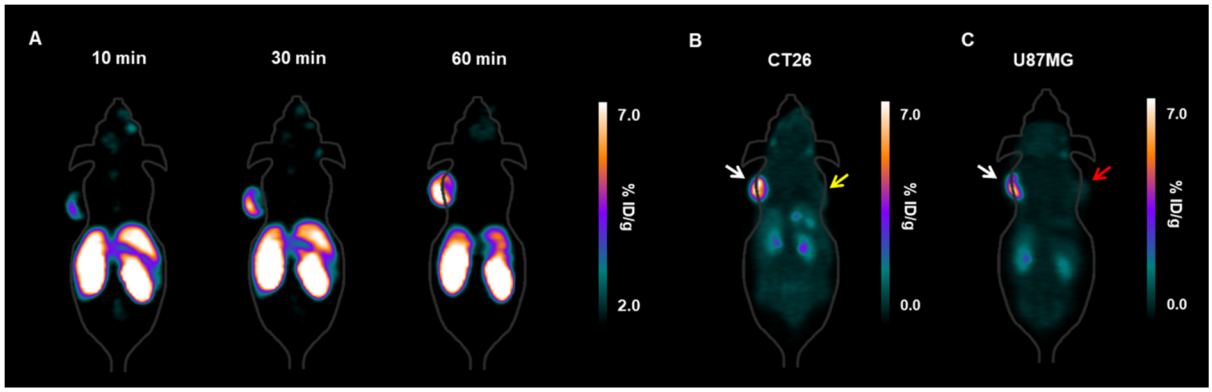

FIGURE 3. (A) MicroPET images of mice bearing B16F10 at 10, 30 and 60 min after injection of ^{18}F-DMFB. (B and C) MicroPET images of mice bearing B16F10 and CT26 (B), and B16F10 and U87MG (C) at 60 min post-injection of ^{18}F-DMFB (white arrow: B16F10; yellow arrow: CT26; red arrow: U87MG).

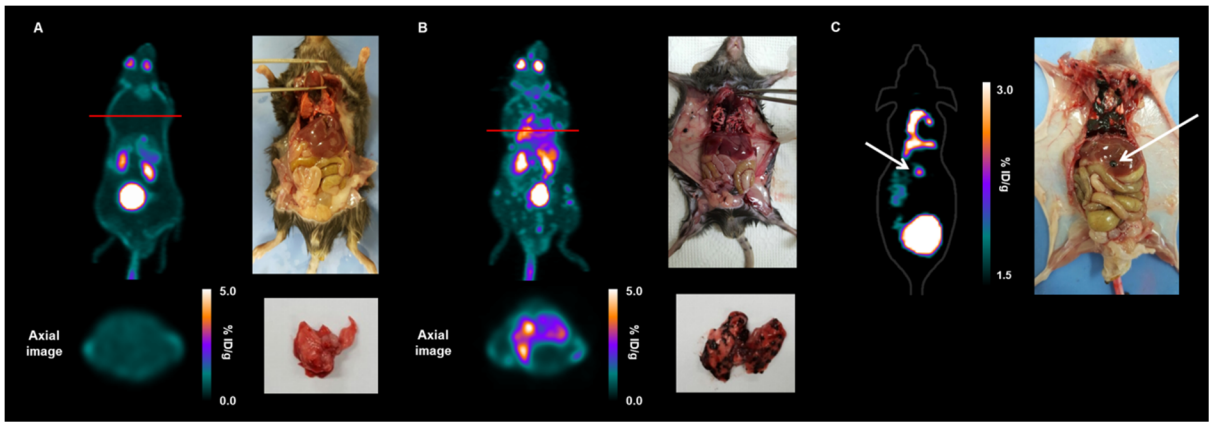

FIGURE 4. Maximum intensity projection (MIP) (upper) and transaxial (lower) images of a (A) normal and (B) lung metastasis model (C57BL/6) at 60 min post-injection of ^{18}F-DMFB. (C) Coronal microPET image of a B16F10 liver metastasis model (Foxn1nu) at 60 min post-injection of ^{18}F-DMFB.

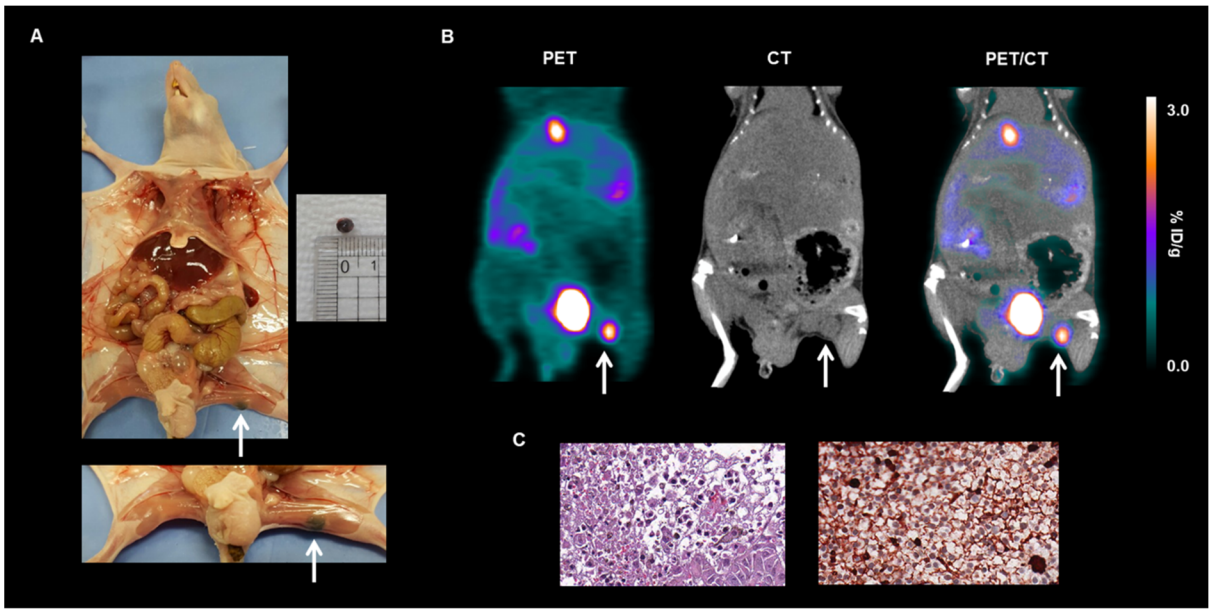

FIGURE 5. (A) Photograph of a B16F10 LN metastasis model. (B) MicroPET, CT and PET/CT fusion images of a B16F10 LN metastasis model at 60 min post-injection of ^{18}F-DMFB (white arrow: LN metastasis region). (C) Pathological examination of a LN metastasis.

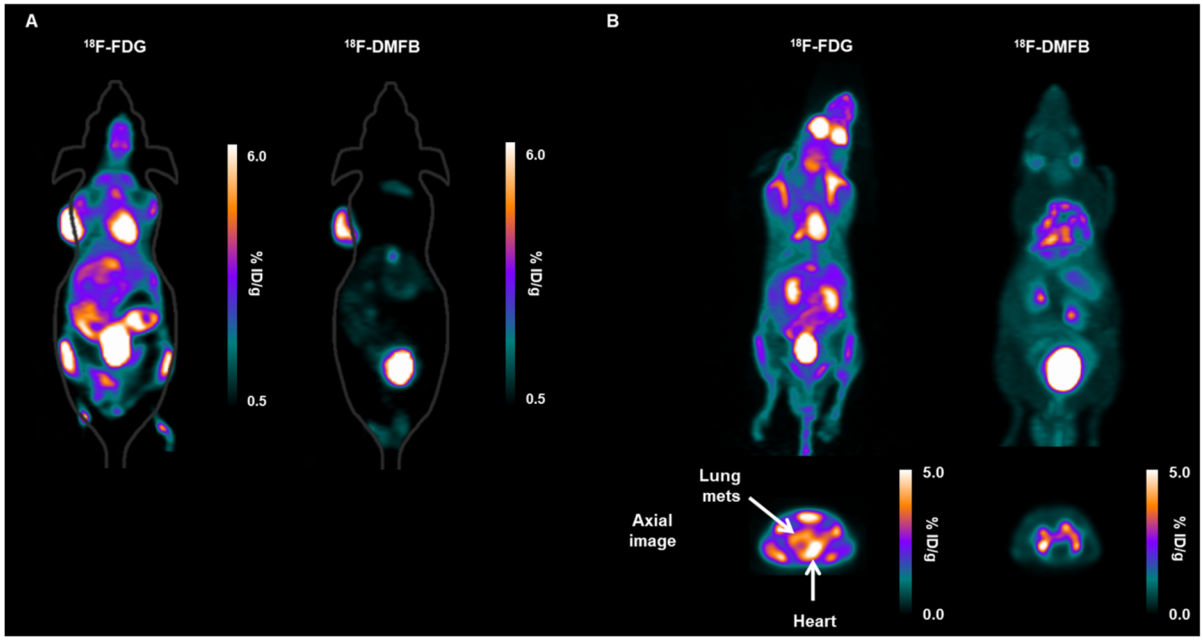

FIGURE 6. MicroPET imaging of ^{18}F-FDG and ^{18}F-DMFB in mice bearing B16F10. (A) Coronal images at 60 min post-injection. (B) MIP (upper) and transaxial (lower) image at 60 min post-injection.

Supplemental Materials

N-(2-(dimethylamino)ethyl)-4-^{18}F-fluorobenzamide: A Novel Molecular Probe for High-Contrast PET Imaging of Malignant Melanoma

Ayoung Pyo[1], Hyeon-Sik Kim[1], Gyeongmin Kim[1], Hyung-Seok Kim[2], Misun Yun[3],

Dong-Yeon Kim[1*], Jung-Joon Min[1*]

[1]*Department of Nuclear Medicine, Chonnam National University Medical School and Hwasun Hospital, Hwasun, Korea*
[2]*Department of Forensic Medicine, Chonnam National University Medical School, Hwasun, Korea*
[3]*Microbiology and Functionality Research Group, World Institute of Kimchi, Gwangju, Korea.*

Address correspondence to: **Jung-Joon Min** (jjmin@jnu.ac.kr), **Dong-Yeon Kim** (blueburr@gmail.com)

Jung-Joon Min, M.D., PhD.
Department of Nuclear Medicine, Chonnam National University Medical School and Hwasun Hospital
160 Ilsimri, Hwasun, Jeonnam 519-763, Republic of Korea
Phone: 82-61-379-2876
Fax: 82-61-379-2875
E-mail: jjmin@jnu.ac.kr

Dong-Yeon Kim, PhD.
Department of Nuclear Medicine, Chonnam National University Medical School and Hwasun Hospital
160 Ilsimri, Hwasun, Jeonnam 519-763, Republic of Korea
Phone: 82-61-379-2872
Fax: 82-61-379-2875
E-mail: blueburr@gmail.com

Ayoung Pyo, PhD
Department of Nuclear Medicine, Chonnam National University Hwasun Hospital
160 Ilsimri, Hwasun, Jeonnam 519-763, Republic of Korea
Tel: 82-61-379-7262
Fax: 82-61-379-2875
E-mail: payjal@naver.com

Short running title: ^{18}F-DMFB for malignant melanoma

Table of Contents

Information	Page
Synthesis scheme for ^{19}F-DMFB (Supplemental Figure 1)	S2
Synthesis scheme for ^{18}F-DMFB (Supplemental Figure 2A)	S2
^{1}H and ^{13}C NMR spectrum of ^{19}F-DMFB (Supplemental Figure 2B and 2C)	S3
Chromatogram of ^{18}F-DMFB separation and analysis (Supplemental Figure 3)	S4
Stability of ^{18}F-DMFB in human serum (Supplemental Figure 4)	S4
Uptake value of ^{18}F-DMFB in normal lung and lung metastasis (Supplemental Figure 5)	S5
MicroPET, CT and PET/CT fusion images of a B16F10 LN metastasis model (Supplemental Figure 6)	S5

Tumro-to-organ ratios of ^{18}F-DMFB in a B16F10 tumor-bearing mouse model (Supplemental Table 1)	S6

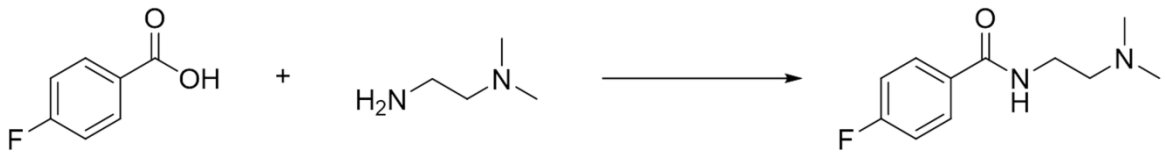

Supplemental Figure 1. Synthesis scheme for ^{19}F-DMFB.

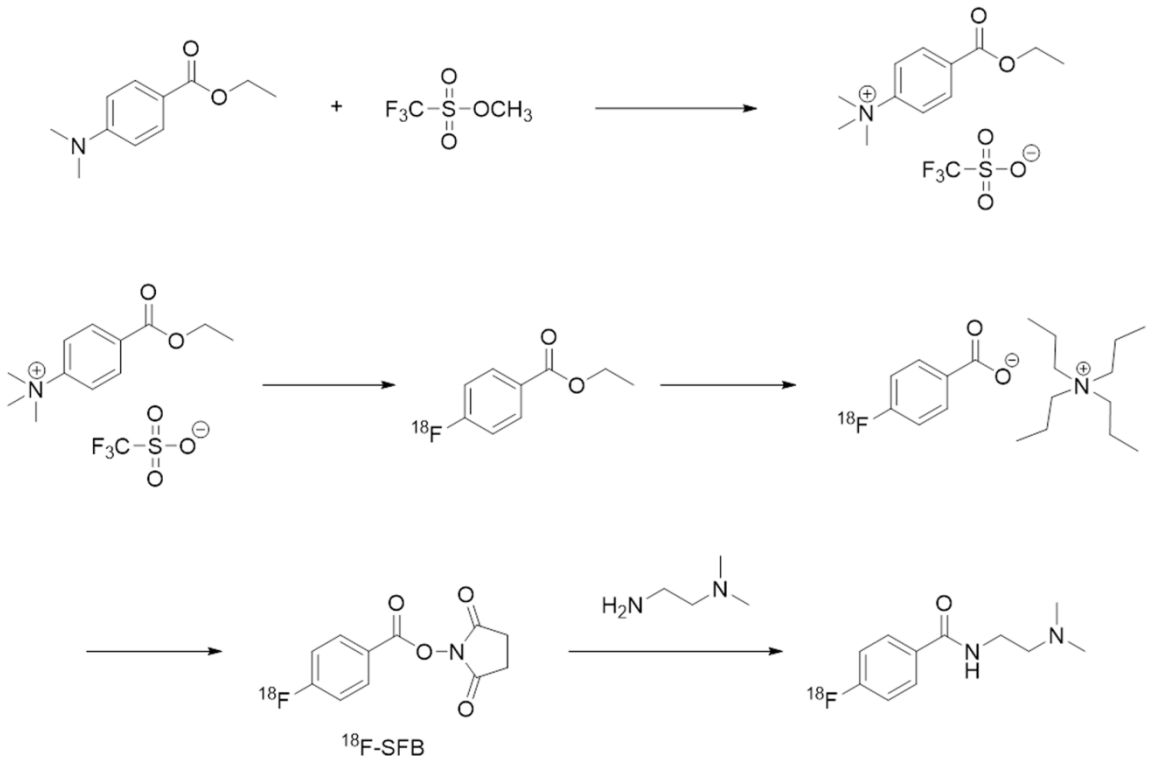

Supplemental Figure 2A. Synthesis scheme for ^{18}F-DMFB.

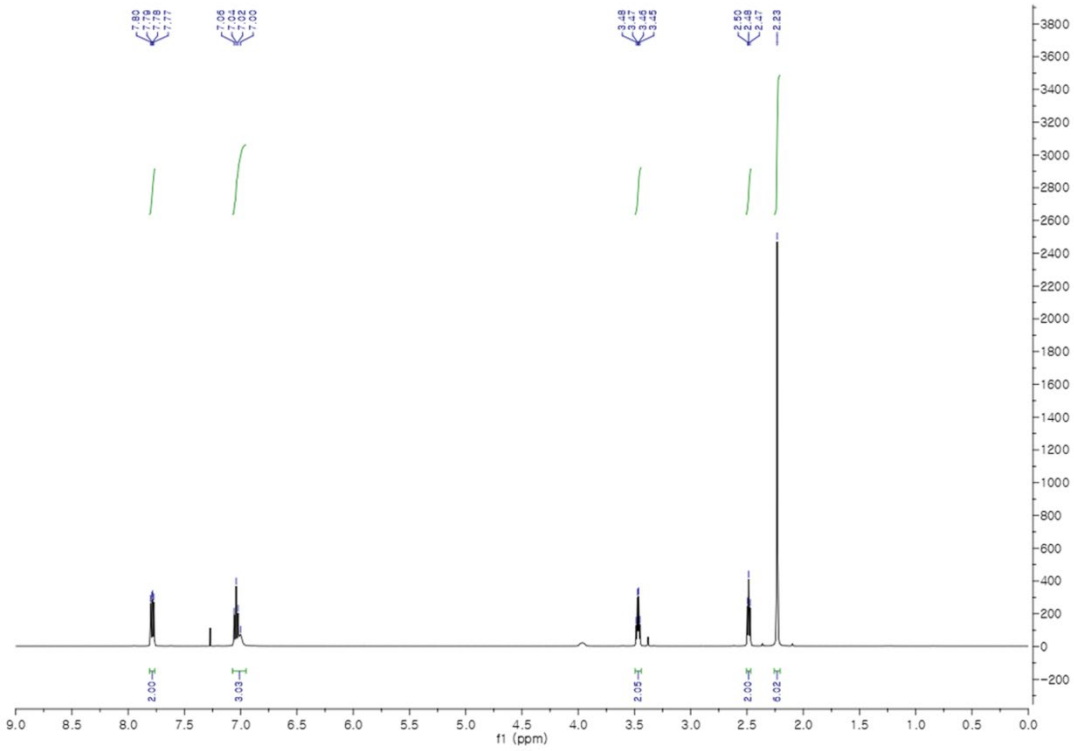

Supplemental Figure 2B. ^{1}H NMR spectrum of ^{19}F-DMFB.

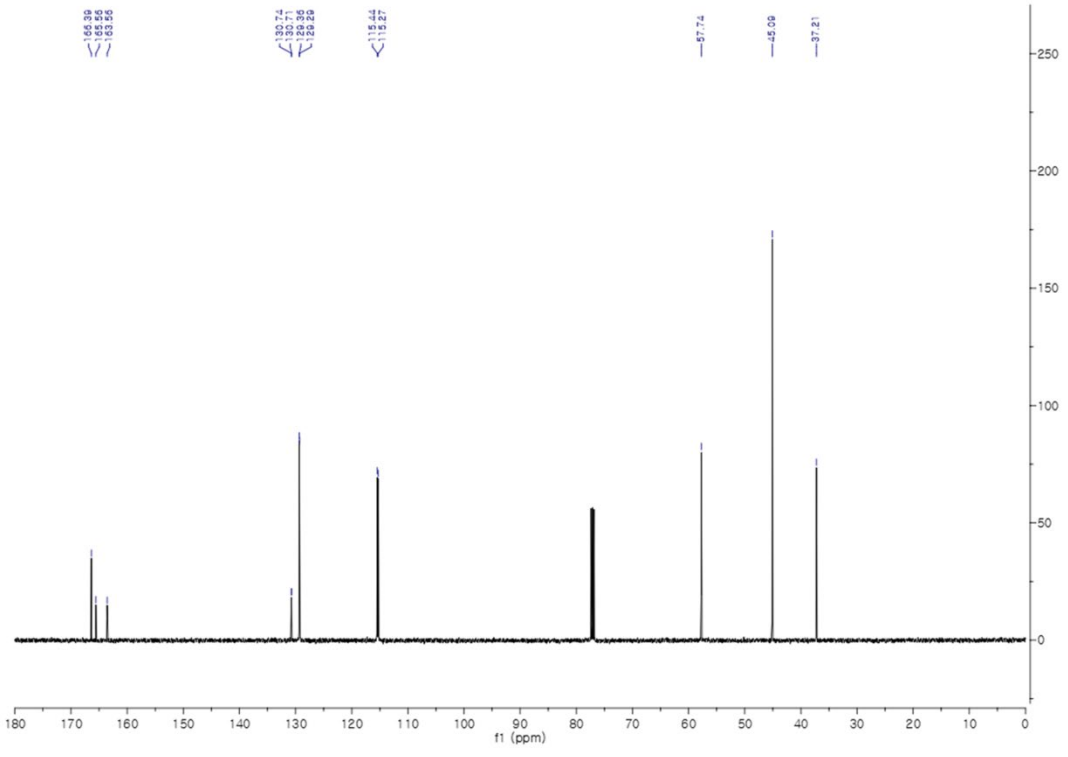

Supplemental Figure 2C. ^{13}C NMR spectrum of ^{19}F-DMFB.

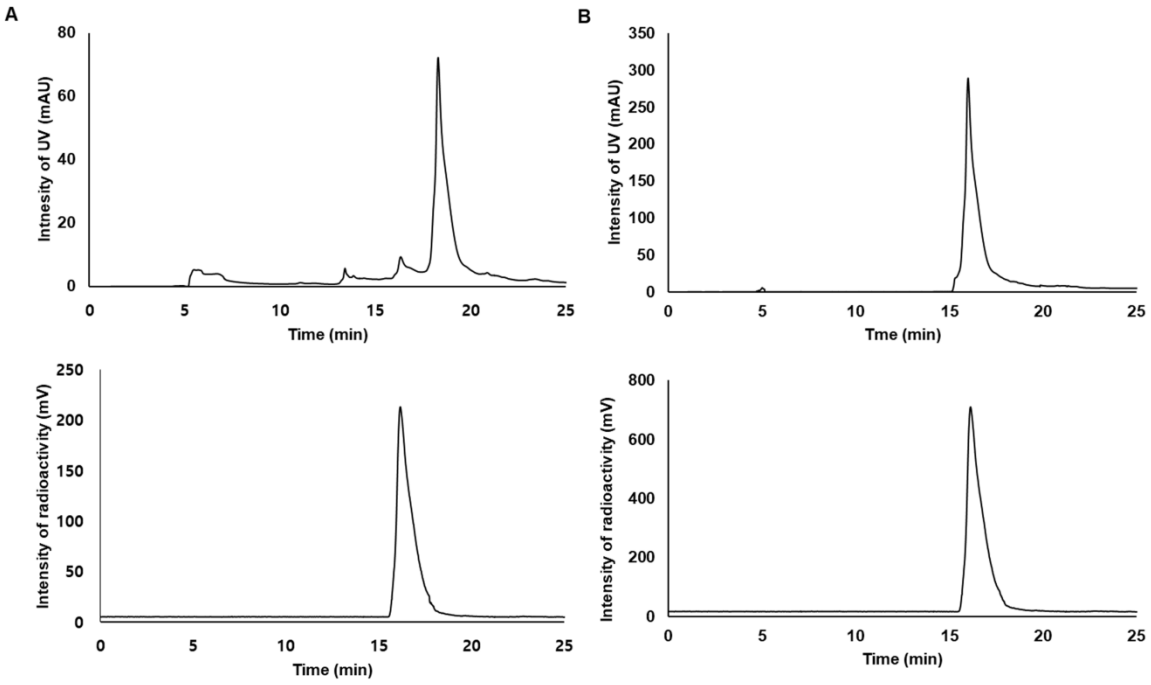

Supplemental Figure 3. (A) Purification of ^{18}F-DMFB using semi-preparative HPLC. (B) HPLC chromatogram of ^{18}F-DMFB, with its non-radioactive compound.

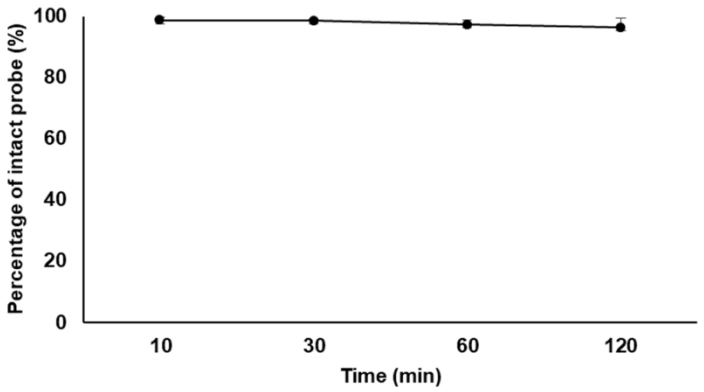

Supplemental Figure 4. ^{18}F-DMFB stability in human serum after incubation at 37 ℃ for 10, 30, 60 and 120 min.

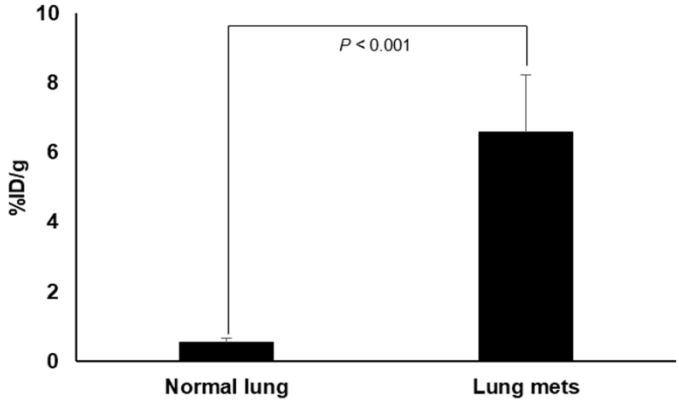

Supplemental Figure 5. Uptake value in normal lung and lung metastasis at 60 min after ^{18}F-DMFB injection.

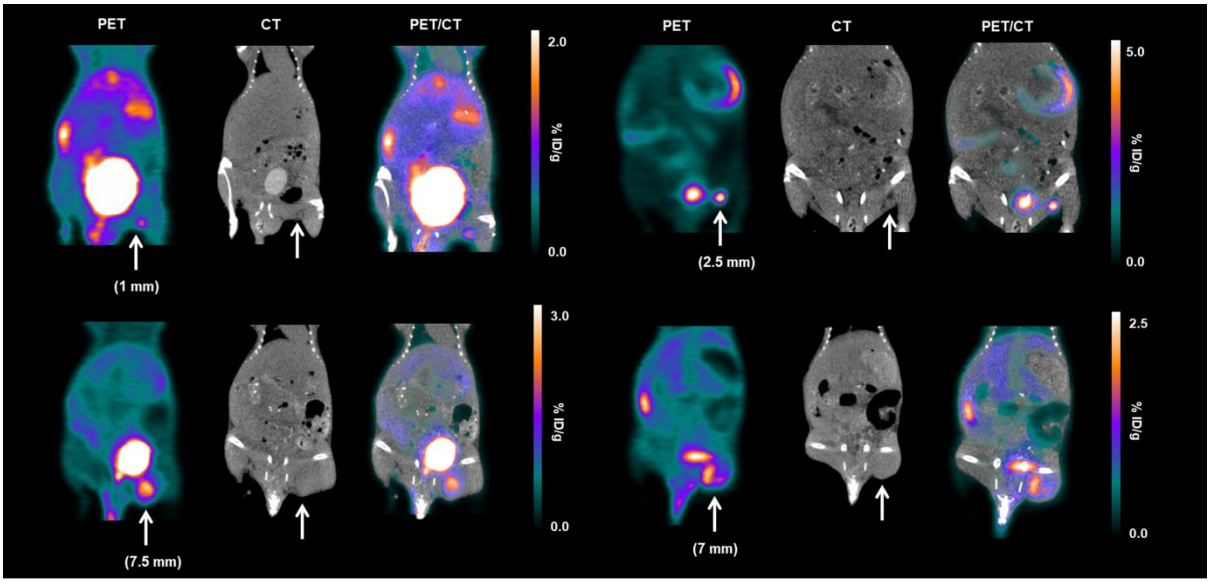

Supplemental Figure 6. MicroPET, CT and PET/CT fusion images of a B16F10 LN metastasis model at 60 min post-injection of ^{18}F-DMFB (white arrow: LN metastasis region).

Supplemental Table 1. Tumro-to-organ ratios of ^{18}F-DMFB in a B16F10 tumor-bearing Foxn1nu mouse model at 10, 30, 60 and 120 min after *i.v.* injection (n = 3 / each time point)

	10 min	**30 min**	**60 min**	**120 min**
Tumor-to-lung	0.85 ± 0.41	2.37 ± 0.63	7.13 ± 2.44	31.81 ± 5.87
Tumor-to-liver	0.83 ± 0.24	1.90 ± 0.66	5.54 ± 1.27	23.73 ± 2.24
Tumor-to-intestine	0.75 ± 0.22	1.39 ± 0.47	4.90 ± 0.22	20.76 ± 3.67
Tumor-to-bone	1.82 ± 0.45	4.47 ± 0.93	13.73 ± 5.87	
Tumor-to-brain	1.40 ± 0.55	3.83 ± 1.62	12.20 ± 5.00	43.40 ± 13.43
Tumor-to-skin	1.28 ± 0.60	2.79 ± 0.91	6.54 ± 1.02	28.99 ± 2.05